Crowding-Regulated Binding of Divalent Biomolecules

Tomasz Skóra,[1,2] Mathijs Janssen,[3,4,5] Andreas Carlson,[3] and Svyatoslav Kondrat[1,6]
[1]Institute of Physical Chemistry, Polish Academy of Sciences, 01-224 Warsaw, Poland
[2]Scientific Computing and Imaging Institute, University of Utah, Salt Lake City, Utah 84112, USA
[3]Department of Mathematics, Mechanics Division, University of Oslo, N-0851 Oslo, Norway
[4]Centre for Cancer Cell Reprogramming, Faculty of Medicine, University of Oslo, Montebello, N-0379 Oslo, Norway
[5]Norwegian University of Life Sciences, Faculty of Science and Technology, Pb 5003, 1433 Ås, Norway
[6]Institute for Computational Physics, University of Stuttgart, Stuttgart 70569, Germany

(Received 6 November 2022; accepted 8 May 2023; published 22 June 2023)

Macromolecular crowding affects biophysical processes as diverse as diffusion, gene expression, cell growth, and senescence. Yet, there is no comprehensive understanding of how crowding affects reactions, particularly multivalent binding. Herein, we use scaled particle theory and develop a molecular simulation method to investigate the binding of monovalent to divalent biomolecules. We find that crowding can increase or reduce cooperativity—the extent to which the binding of a second molecule is enhanced after binding a first molecule—by orders of magnitude, depending on the sizes of the involved molecular complexes. Cooperativity generally increases when a divalent molecule swells and then shrinks upon binding two ligands. Our calculations also reveal that, in some cases, crowding enables binding that does not occur otherwise. As an immunological example, we consider immunoglobulin G-antigen binding and show that crowding enhances its cooperativity in bulk but reduces it when an immunoglobulin G binds antigens on a surface.

DOI: 10.1103/PhysRevLett.130.258401

Introduction.—The intracellular space of living cells is crowded by biomacromolecules—in *Escherichia coli*, for instance, up to 44% [1–3]. These macromolecular "crowders" can affect biophysical processes through the volume they exclude: *Crowding* [4–7] can hinder diffusion [8–10], promote association reactions [11–13], shift equilibria in the direction of smaller and more spherical conformations of reacting species [14,15], enhance or reduce enzyme-catalyzed reactions [16–19], etc. As a result, crowding affects physiological processes like senescence [20], gene regulation [21], and cell growth [22].

Biochemical reactions often involve macromolecules with more than one binding site [23–26]. Examples of *multivalent binding* include hemoglobin binding four oxygen molecules [27,28], antibodies binding two antigens [29], the condensation of multivalent intrinsically disordered proteins [30,31], and multivalent binding in synthetic systems [32,33]. Multivalent binding can be *cooperative*, meaning that the association constant of each further binding step is larger than that of the previous step [23,34]. Cooperative systems show "on-off behavior" where multivalent molecules change from being unbound to being fully bound upon slight changes in, e.g., ligand concentration or temperature; noncooperative systems behave more gradually. Correspondingly, the concentration of partly bound multivalent particles is smaller for more cooperative binding reactions. One speaks of *allosteric* cooperativity when the binding interactions are intermolecular, as is the case, for instance, with oxygen-hemoglobin binding. Conversely, the cooperativity of intramolecular interactions is called *chelate* [25].

Despite the biological importance of molecules with multiple binding sites, how crowding affects multivalent binding is yet to be investigated theoretically (see, however, Ref. [35]). Herein, we use scaled particle theory (SPT) and develop a general molecular simulation method to study how physiologically relevant crowding conditions affect divalent binding. We find that crowding can enhance or reduce cooperativity depending on the size differences between reactants and products, in some cases enabling divalent binding *per se*. With molecular simulations of a coarse-grained immunoglobulin G (IgG) model, we show that IgG-antigen binding cooperativity depends sensitively on whether it occurs in bulk or on a surface.

Divalent binding.—We consider a divalent molecule AA that reversibly binds two B molecules [Fig. 1(a)]:

$$AA + B \overset{2K_1}{\rightleftharpoons} AA \cdot B, \tag{1a}$$

$$AA \cdot B + B \overset{\frac{1}{2}K_2}{\rightleftharpoons} AA \cdot B_2, \tag{1b}$$

where K_1 and K_2 are equilibrium constants of the individual binding events. We denote by $[AA]$ and $[B]$ the equilibrium concentrations of unbound AA and B

molecules, respectively, and by $[AA]_T = [AA] + [AA \cdot B] + [AA \cdot B_2]$ and $[B]_T = [B] + [AA \cdot B] + 2[AA \cdot B_2]$ their total concentrations, where $[AA \cdot B]$ and $[AA \cdot B_2]$ are the equilibrium concentrations of $AA \cdot B$ and $AA \cdot B_2$ complexes, respectively. The reaction-rate equations associated with Eq. (1) are a set of four coupled ordinary differential equations for the time-dependent concentrations of the four molecular species. At steady state, these equations can be reduced to a single cubic equation for $[AA \cdot B]$ (see Ref. [24]) or $[B]$ (see Refs. [36,37]) in terms of K_1, K_2, $[AA]_T$, and $[B]_T$. The solutions to these cubic equations then allow one to find the concentrations of the other species (Sec. S1 in Ref. [38]).

If the above reaction happens among chemically inert crowders, the association constants amount to

$$K_1(\phi) = \frac{1}{2}\frac{[AA \cdot B]}{[AA][B]} = K_1(0)\frac{\gamma_{AA}\gamma_B}{\gamma_{AA \cdot B}}, \tag{2a}$$

$$K_2(\phi) = 2\frac{[AA \cdot B_2]}{[AA \cdot B][B]} = K_2(0)\frac{\gamma_{AA \cdot B}\gamma_B}{\gamma_{AA \cdot B_2}}, \tag{2b}$$

where ϕ is the volume fraction occupied by crowders and γ_i is the activity coefficient of species $i \in \{AA, B, AA \cdot B, AA \cdot B_2\}$. We use the allosteric cooperativity factor $\alpha = K_2/K_1$ [23] and speak of cooperative binding when $\alpha > 1$. With Eq. (2), we find

$$\frac{\alpha}{\alpha_0} = \frac{\gamma_{AA \cdot B}^2}{\gamma_{AA}\gamma_{AA \cdot B_2}}, \tag{3}$$

where $\alpha_0 = K_2(0)/K_1(0)$ is the cooperativity factor in the absence of crowders. If, instead of two monovalent B molecules, AA binds another divalent molecule BB, the second binding step is intramolecular. For this case, the chelate cooperativity factor is $\alpha = K_2/(2[BB]K_1)$ [25], yielding the same expression for α/α_0 but with a different α_0. In the following, we consider $[AA]_T$ and $[B]_T$ much smaller than the concentration of crowders and study how crowding affects cooperativity by computing activity coefficients as functions of ϕ.

SPT results.—As a starting point, we use SPT, which offers approximate analytical expressions for the activity coefficients of macromolecules and macromolecular complexes of convex shapes. A protein-ligand complex can have a larger [50,51] or a smaller [52–61] radius of gyration than the corresponding unbound protein. Accordingly, in our model, we consider AA, $AA \cdot B$, and $AA \cdot B_2$ complexes to be spheres of radii R_{AA}, $R_{AA \cdot B} = R_{AA} + \delta R_1$, and $R_{AA \cdot B_2} = R_{AA \cdot B} + \delta R_2$, respectively [Fig. 1(a)], where δR_1 and δR_2 can be positive or negative. Assuming also crowders to be spheres of equal radius R_c, we can estimate the activity coefficients γ_i with Minton's generalized SPT [5] (Sec. S2 A in Ref. [38]):

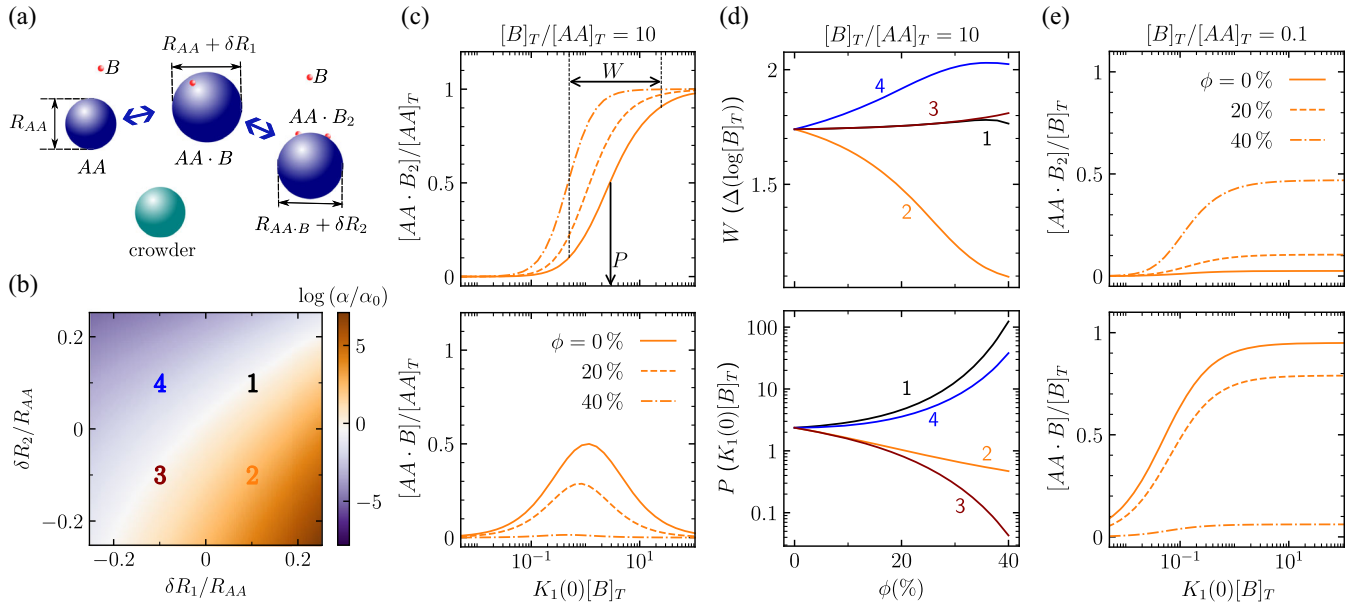

FIG. 1. Divalent binding with crowding dependence through SPT. (a) Schematic of a divalent molecule AA that binds two monovalent molecules B, indicating the sizes of the different macromolecular complexes. (b) Heat map of $\log(\alpha/\alpha_0)$ plotted in the plane of $\delta R_1/R_{AA}$ and $\delta R_2/R_{AA}$ for an occupied volume fraction $\phi = 40\%$, AA size $R_{AA} = 6$ nm, and crowder size $R_c = 5.1$ nm (corresponding to Ficoll 70, a typical synthetic crowder). The colored numbers (1–4) indicate the values of $\delta R_1 = \pm 0.1 R_{AA}$ and $\delta R_2 = \pm 0.1 R_{AA}$ used in the other panels. (c) Dependence of $[AA \cdot B_2]$ and $[AA \cdot B]$ on the concentration of B molecules. The concentration $[B]_T/[AA]_T = 10$ and $\delta R_1 = -\delta R_2 = 0.1 R_{AA}$ [point 2 in (b)]. (d) The width and position of the $[AA \cdot B_2]$ profile [cf. (c)] for $[B]_T/[AA]_T = 10$ and for four combinations of $\delta R_1 = \pm 0.1$ and $\delta R_2 = \pm 0.1$ corresponding to the points in (b). (e) Dependence of $[AA \cdot B_2]$ and $[AA \cdot B]$ on the concentration of B molecules for $[B]_T/[AA]_T = 0.1$ and $\delta R_1 = -\delta R_2 = 0.1 R_{AA}$ [point 2 in (b)].

$$\ln\gamma_i(\phi) = \ln(1+g) + g\left(\frac{3R_i}{R_c} + \frac{3R_i^2}{R_c^2} + \frac{R_i^3}{R_c^3}\right) + \frac{g^2}{2}\left(\frac{9R_i^2}{R_c^2} + \frac{6R_i^3}{R_c^3}\right) + 3g^3\frac{R_i^3}{R_c^3}, \quad (4)$$

where $g(\phi) = \phi/(1-\phi)$. We combine Eqs. (3) and (4) to draw a heat map [Fig. 1(b)] of $\log(\alpha/\alpha_0)$ (base 10) in the plane of δR_1 and δR_2 for $\phi = 40\%$. We see that AA particles that swell and then shrink upon binding two B particles (point 2) have an enhanced cooperativity. By contrast, AA particles that shrink and then swell (point 4) have a decrease in cooperativity. The cooperativity of particles that swell twice (point 1) or shrink twice (point 3) is hardly affected by crowders. Intuitively, excluded-volume interactions with crowders become more important for larger molecules, because they leave less space for the crowders. In the case of point 2, with intermediates $AA\cdot B$ being larger than AA and $AA\cdot B_2$, crowder-molecule interactions will suppress $[AA\cdot B]$, driving up $[AA]$ and $[AA\cdot B_2]$. Hence, $K_1(\phi)$ decreases and $K_2(\phi)$ increases with ϕ, explaining the $\log(\alpha/\alpha_0) > 0$ value observed. Similar reasoning explains the trends at points 1, 3, and 4.

Next, we calculate binding curves of $[AA\cdot B_2]/[AA]_T$ and $[AA\cdot B]/[AA]_T$ versus the scaled density $K_1[B]_T$ at fixed $[B]_T/[AA]_T$. These curves represent numerical solutions to the cubic equation mentioned below Eq. (1) [see Eq. (S6) in Ref. [38]]—we again used Minton's theory to determine $K_1(\phi)$ and $K_2(\phi)$. Figure 1(c) concerns a case where B molecules outnumber AA molecules, $[B]_T/[AA]_T = 10$. We also set $\delta R_1 = 0.1R_{AA}$ and $\delta R_2 = -0.1R_{AA}$, corresponding to point 2 in Fig. 1(b). The $[AA\cdot B_2]/[AA]_T$ profile has a typical sigmoidal shape that shifts toward smaller $K_1(0)[B]$ with increasing ϕ. The sigmoid also becomes steeper with ϕ, which is the on-off behavior typical of cooperative systems mentioned in the introduction. Moreover, $[AA\cdot B]$ decreases with crowding—at the highest $\phi = 40\%$ considered, there are practically no intermediates $AA\cdot B$ at any concentration of monovalent molecules [bottom plot in Fig. 1(c)].

To characterize a $[AA\cdot B_2]/[AA]_T$ curve, we define the position P of its midpoint as the $K_1(0)[B]$ value at which the derivative $d[AA\cdot B_2]/d[B]_T$ is maximal. We also define the profile width W as the difference in the $K_1(0)[B]$ values at which the concentrations $[AA\cdot B_2]/[AA]_T$ are $10/11$ and $1/11$ of the maximum (i.e., $[AA]_T$). Note that W is similar to the switching window of Hunter and Anderson [23], which dealt with the total concentration of bound molecules (i.e., the sum of $[AA\cdot B_2]$ and $[AA\cdot B]$) instead. In Fig. 1(c) (top panel), W decreases with crowding, in line with the increased cooperativity at point 2 in Fig. 1(b). The position P decreases with increasing ϕ, because crowders tend to promote binding: For given $K_1[B]_T$, a larger fraction of AA particles are in the fully bound state $AA\cdot B_2$.

Figure 1(d) shows P and W versus ϕ for the four combinations of δR_1 and δR_2 indicated with numbers 1–4 in Fig. 1(b). The panel for W corroborates our Fig. 1(b) findings: W varies inversely with the change α/α_0 in cooperativity, where molecules that swell and shrink have large α/α_0, and hence their W decreases. Molecules for which $\delta R_1 = \delta R_2$ (points 1 and 3) showed no change in cooperativity in Fig. 1(b), and, likewise, their window W versus ϕ is roughly constant. Interestingly, the positions P of their binding curves show opposing trends. The conventional wisdom of crowders driving reactions toward the bound state (i.e., decreasing P) does not hold for divalent molecules that continually swell upon binding and is, thus, not correct, in general. This conclusion is in line with a recent study by Schreck, Bridstrup, and Yuan [12] on protein folding and aggregation.

Lastly, Fig. 1(e) shows binding curves for the same settings as in Figs. 1(c) and 1(d) except $[B]_T/[AA]_T = 0.1$; hence, AA now outnumber B molecules. In the absence of crowders and for large $K_1(0)[B]$, the system is saturated with intermediates $AA\cdot B$, while the concentration of $AA\cdot B_2$ practically vanishes. This situation changes when the occupied volume fraction ϕ of crowders increases, especially for the physiologically relevant value 40%. In that case, the concentration of fully bound complexes $AA\cdot B_2$ reaches values close to the maximum $[AA\cdot B_2] \approx 0.5[B]_T$, while the concentration of intermediates almost vanishes. This behavior is because crowders enhance cooperativity (for $\delta R_1 = -\delta R_2 = 0.1R_{AA}$ as considered here), and, in turn, cooperativity promotes fully bound complexes. Hence, when AA molecules outnumber B molecules, crowding enables divalent binding.

Activity coefficients from molecular simulations.—SPT is limited to convex shapes and breaks down for large volume fractions and small crowders. Here, based on Ref. [62], we develop a method for numerically calculating activity coefficients in crowded media with Monte Carlo (MC) and Brownian dynamics (BD) simulations. We consider a molecule of species i to comprise n_i beads. When such a molecule is among N_c crowders at positions $\{\boldsymbol{R}_k\}$, its activity coefficient reads [39,62] (Sec. S2 in Ref. [38])

$$\gamma_i^{-1}(\{\boldsymbol{R}_k\}) = Z_i(\{\boldsymbol{R}_k\})Z_i^{-1}(\varnothing), \quad (5a)$$

where $\{\boldsymbol{R}_k\} = \varnothing$ signifies the absence of crowders and

$$Z_i(\{\boldsymbol{R}_k\}) = \int\prod_{j=1}^{n_i} d\boldsymbol{r}_j \exp\left[-\beta\mathcal{U}_i(\{\boldsymbol{r}_j\})\right] \times \exp\left[-\beta\sum_{j=1}^{n_i}\sum_{k=1}^{N_c} U(\boldsymbol{r}_j - \boldsymbol{R}_k)\right] \quad (5b)$$

is the configurational partition function of the molecule, where $\mathcal{U}_i$ is the intramolecular potential energy of species i and $U(\boldsymbol{r}_j - \boldsymbol{R}_k)$ is the interaction energy of crowder k with bead j at position $\boldsymbol{r}_j$. To calculate the integral in Eq. (5b)

through the MC method, we reduce it to (Sec. S2 B in Ref. [38])

$$\gamma_i^{-1}(\{\boldsymbol{R}_k\}) \approx \frac{1}{M}\sum_{\alpha=1}^{M} \exp\left[-\beta \sum_{j=1}^{n_i}\sum_{k=1}^{N_c} U(\boldsymbol{r}_j^{(\alpha)} - \boldsymbol{R}_k)\right], \quad (6)$$

where α in $\boldsymbol{r}_j^{(\alpha)}$ denotes an MC draw with conformations (i.e., $\boldsymbol{r}_j^{(\alpha)}$) obtained from BD simulations of single molecule i and M is the total number of draws (Sec. S2 C in Ref. [38]). To obtain the activity coefficient in a crowded system, we average over the distribution of crowders, $\gamma_i^{-1} = \langle \gamma_i^{-1}(\{\boldsymbol{R}_k\})\rangle_c$, where we used BD simulation to obtain crowder configurations in the absence of molecule i (Sec. S2 D in Ref. [38]).

While this approach is general, in all our calculations below, we consider only hard-sphere interactions $U = U_{\mathrm{HS}}$ [see Eq. (S20) in Ref. [38]] between beads and crowders. In this case, we have $\gamma_i^{-1} = V_{\mathrm{acc},i}/V$, with V the volume of the system and $V_{\mathrm{acc},i}$ the average volume accessible to molecule i, that is, not excluded by crowders. Thus, the activity of the molecular species i is $a_i \equiv \gamma_i[i] = N_i/V_{\mathrm{acc},i}$, where N_i is the number of molecules i.

Polymer bead models of divalent molecules.—Polymer bead chains are simplistic models of macromolecules in which ring-forming end-to-end reactions may represent the folding of protein or single-stranded DNA or other conformational changes [63]. We consider a cyclic AA molecule of n_{AA} beads that opens to bind a first B molecule and closes again after binding another B molecule [Fig. 2(a)]. Figure 2(b) shows the gyration radii of the AA, $AA \cdot B$, and $AA \cdot B_2$ molecule complexes. For $n_{AA} > 2$, an AA first swells and then shrinks upon binding two B molecules [64]. This case, therefore, corresponds to point 2 in Fig. 1(b), for which SPT predicted enhanced cooperativity. Simulation results shown in Figs. 2(c) and 2(d) confirm that the cooperativity increases with crowding for all polymer lengths. The magnitude of the observed crowding-induced cooperativity change increases with increasing AA length, likely because the differences in the gyration radii increase with the number of beads. We also studied linear AA polymers and AA polymers binding to divalent BB particles and again found increasing cooperativity with increasing AA length (Figs. S4 and S5 in Ref. [38]).

Unlike the models we have discussed so far, the cytoplasm contains crowders of various shapes and sizes. To account for polydispersity in size, we use a mixture of spherical crowders of different radii modeled after the cytoplasm of *E. coli* [40]. For this cytoplasm model, cooperativity of divalent binding again increases with the AA length [Fig. 2(c)]. For the largest AA considered (30 beads), the reaction is more than 7 times more cooperative inside the cytoplasm than in infinite dilution. Note a crossover between the cooperativities in the cytoplasm ($\phi \approx 42.6\%$) and the most crowded Ficoll 70 system ($\phi \approx 44.2\%$). A similar crossover has been reported in the case of macromolecular diffusion [65], underlining the importance of the composition of a crowded environment [66–68].

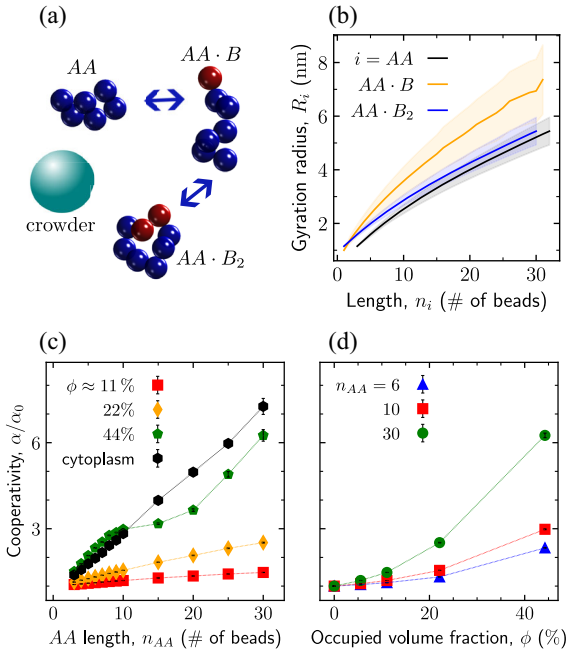

FIG. 2. Cooperativity from simulations. (a) Schematic of the binding of a monovalent molecule B (red beads) to a divalent molecule AA (composed of blue beads). In the first step, a cyclic AA opens to bind B; in the second step, AA binds a second B molecule and closes to become a ring again. (b) Gyration radii of various complexes. (c),(d) Cooperativity as a function of (c) AA length and (d) occupied volume fraction ϕ. The bead radius is 1 nm, and the crowder radius is $R_c = 5.1$ nm, corresponding to Ficoll 70. For the cytoplasm, $\phi \approx 42.6\%$.

IgG-antigen binding.—After these generic considerations, we focus on a biologically relevant example of divalent binding of IgG, which is one of the most common types of antibody. IgG is a Y-shaped protein, each tip of which binds to the antigen of a microbe or infected cell. To determine how crowders affect IgG-antigen binding, we use a coarse-grained IgG model, which we introduce in an upcoming article [41] (see Sec. S3 in Ref. [38]). This model reproduces the experimentally measured angle distributions [42] and hydrodynamic radius of IgG [9]. Since IgG binds to antigens on the surface of a pathogen, we consider divalent binding at a flat surface. For comparison, however, we first evaluate the cooperativity of IgG-antigen binding in bulk, both for unconstrained antigens and when two antigens are at different fixed separations ℓ (the latter yields a system with chelate cooperativity). In all cases, the cooperativity increases with crowding [Fig. 3(b), full triangles], similar to the polymer bead model considered above. The cooperativity increases most for small ℓ, likely because the crowders squeeze an IgG, making it more likely to bind antigens connected at smaller separations.

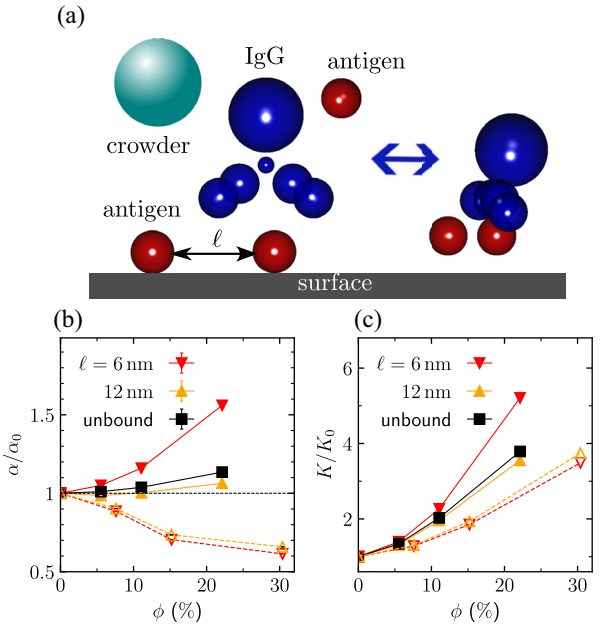

FIG. 3. IgG-antigen binding in crowded environments. (a) Schematics showing a model IgG, antigens, and a crowder. An IgG binds to antigens by two flexible arms modeled by two beads each. We consider binding in bulk and at a surface. (b) Cooperativity for IgG-antigen binding as a function of the occupied volume fraction of crowders ϕ. The results for binding in bulk and on a surface are shown by full and open symbols with the same color code, respectively. (c) The same as (b) but for the total equilibrium constant.

Unlike in bulk, the IgG-antigen cooperativity decreases when the binding occurs at a surface [Fig. 3(b), open triangles]. Arguably, crowding promotes the binding of a first antigen because an IgG-antigen complex at the surface excludes less volume than a similar complex in bulk; the same mechanism does not promote the binding of a second antigen, as the partially bound IgG is already at the surface (Fig. S6 in Ref. [38]). The equilibrium constant K_1 thus increases with crowding more than K_2, and, hence, $\alpha = K_2/K_1$ decreases. Still, we observe an increase in the total equilibrium constant $K = K_1K_2$ in all cases [Fig. 3(c)], in line with the traditional view that crowding enhances association.

Conclusion.—We have studied how crowding affects the binding of a divalent molecule AA to two monovalent molecules B. By using SPT, we found that crowding could enhance or reduce cooperativity, depending on the sizes of the different molecular complexes (Fig. 1). When the AA molecules substantially outnumber the B molecules, divalent binding occurs only in the presence of crowders. We developed a general simulation method to compute activity coefficients under crowded conditions and applied it to bead-chain AA molecules binding to single-bead B molecules (Fig. 2), corroborating our SPT findings. We also studied how crowding affects IgG-antigen binding using coarse-grained models for both molecules. We found opposite trends, where crowding enhances cooperativity for bulk reactions but reduces it when the antibody binds to antigens on a surface. Our results suggest that crowding can substantially affect divalent binding, which we hope stimulates further theoretical and experimental studies. Future work may focus on applying our simulation method to atomistic models of reacting biomolecules and investigating the kinetics of divalent binding in biologically relevant crowded environments.

This work was supported by NCN grant No. 2017/25/B/ST3/02456 to S. K. and T. S. We thank PLGrid for providing computational resources. M. J. was supported by an Advanced Grant from the European Research Council (No. 788954). The research leading to these results has received funding from the European Union's Horizon 2020 research and innovation programme under the Marie Skłodowska-Curie grant agreement No 801133.

[1] K. Luby-Phelps, The physical chemistry of cytoplasm and its influence on cell function: An update, Mol. Biol. Cell **24**, 2593 (2013).
[2] A. P. Minton, How can biochemical reactions within cells differ from those in test tubes?, J. Cell Sci. **128**, 1254 (2015).
[3] S. B. Zimmerman and S. O. Trach, Estimation of macromolecule concentrations and excluded volume effects for the cytoplasm of Escherichia coli, J. Mol. Biol. **222**, 599 (1991).
[4] S. B. Zimmerman and A. P. Minton, Macromolecular crowding: Biochemical, biophysical, and physiological consequences, Annu. Rev. Biophys. Biomol. Struct. **22**, 27 (1993).
[5] A. P. Minton, Molecular crowding: Analysis of effects of high concentrations of inert cosolutes on biochemical equilibria and rates in terms of volume exclusion, Methods Enzymol. **295**, 127 (1998).
[6] R. J. Ellis, Macromolecular crowding: Obvious but underappreciated, Trends Biochem. Sci. **26**, 597 (2001).
[7] M. Feig, I. Yu, P. H. Wang, G. Nawrocki, and Y. Sugita, Crowding in cellular environments at an atomistic level from computer simulations, J. Phys. Chem. B **121**, 8009 (2017).
[8] J. A. Dix and A. S. Verkman, Crowding effects on diffusion in solutions and cells, Annu. Rev. Biophys. **37**, 247 (2008).
[9] N. O. Junker, F. Vaghefikia, A. Albarghash, H. Höfig, D. Kempe, J. Walter, J. Otten, M. Pohl, A. Katranidis, S. Wiegand, and J. Fitter, Impact of molecular crowding on translational mobility and conformational properties of biological macromolecules, J. Phys. Chem. B **123**, 4477 (2019).
[10] T. Skóra, F. Vaghefikia, J. Fitter, and S. Kondrat, Macromolecular crowding: How shape and interactions affect diffusion, J. Phys. Chem. B **124**, 7537 (2020).
[11] A. P. Minton, Influence of macromolecular crowding upon the stability and state of association of proteins: Predictions and observations, J. Pharm. Sci. **94**, 1668 (2005).

[12] J. S. Schreck, J. Bridstrup, and J.-M. Yuan, Investigating the effects of molecular crowding on the kinetics of protein aggregation, J. Phys. Chem. B **124**, 9829 (2020).
[13] L. Heo, Y. Sugita, and M. Feig, Protein assembly and crowding simulations, Curr. Opin. Struct. Biol. **73**, 102340 (2022).
[14] M. S. Cheung, D. Klimov, and D. Thirumalai, Molecular crowding enhances native state stability and refolding rates of globular proteins, Proc. Natl. Acad. Sci. U.S.A. **102**, 4753 (2005).
[15] A. G. Gasic, M. M. Boob, M. B. Prigozhin, D. Homouz, C. M. Daugherty, M. Gruebele, and M. S. Cheung, Critical Phenomena in the Temperature-Pressure-Crowding Phase Diagram of a Protein, Phys. Rev. X **9**, 041035 (2019).
[16] M. G. Norris and N. Malys, What is the true enzyme kinetics in the biological system? An investigation of macromolecular crowding effect upon enzyme kinetics of glucose-6-phosphate dehydrogenase, Biochem. Biophys. Res. Commun. **405**, 388 (2011).
[17] I. Pastor, L. Pitulice, C. Balcells, E. Vilaseca, S. Madurga, A. Isvoran, M. Cascante, and F. Mas, Effect of crowding by Dextrans in enzymatic reactions, Biophys. Chem. **185**, 8 (2014).
[18] K. Maximova, J. Wojtczak, and J. Trylska, Enzymatic activity of human immunodeficiency virus type 1 protease in crowded solutions, Eur. Biophys. J. **48**, 685 (2019).
[19] T. Skóra, M. N. Popescu, and S. Kondrat, Conformation-changing enzymes and macromolecular crowding, Phys. Chem. Chem. Phys. **23**, 9065 (2021).
[20] A. P. Minton, Water loss in aging erythrocytes provides a clue to a general mechanism of cellular senescence, Biophys. J. **119**, 2039 (2020).
[21] M. Tabaka, T. Kalwarczyk, and R. Hołyst, Quantitative influence of macromolecular crowding on gene regulation kinetics, Nucl. Acids Res. **42**, 727 (2014).
[22] B. Alric, C. Formosa-Dague, E. Dague, L. J. Holt, and M. Delarue, Macromolecular crowding limits growth under pressure, Nat. Phys. **18**, 411 (2022).
[23] C. A. Hunter and H. L. Anderson, What is cooperativity?, Angew. Chem., Int. Ed. **48**, 7488 (2009).
[24] M. Janssen, H. Stenmark, and A. Carlson, Divalent ligand-monovalent molecule binding, Soft Matter **17**, 5375 (2021).
[25] G. Ercolani and L. Schiaffino, Allosteric, chelate, and interannular cooperativity: A mise au point, Angew. Chemie., Int. Ed. **50**, 1762 (2011).
[26] A. S. Perelson and C. DeLisi, Receptor clustering on a cell surface. I. Theory of receptor cross-linking by ligands bearing two chemically identical functional groups, Math. Biosci. **48**, 71 (1980).
[27] G. K. Ackers, M. L. Doyle, D. Myers, and M. A. Daugherty, Molecular code for cooperativity in hemoglobin, Science **255**, 54 (1992).
[28] W. A. Eaton, E. R. Henry, J. Hofrichter, and A. Mozzarelli, Is cooperative oxygen binding by hemoglobin really understood?, Nat. Struct. Biol. **6**, 351 (1999).
[29] D. Yang, R. Kroe-Barrett, S. Singh, C. J. Roberts, and T. M. Laue, IgG cooperativity–Is there allostery? Implications for antibody functions and therapeutic antibody development, MAbs **9**, 1231 (2017).
[30] P. Li, S. Banjade, H. C. Cheng, S. Kim, B. Chen, L. Guo, M. Llaguno, J. V. Hollingsworth, D. S. King, S. F. Banani, P. S. Russo, Q. X. Jiang, B. T. Nixon, and M. K. Rosen, Phase transitions in the assembly of multivalent signalling proteins, Nature (London) **483**, 336 (2012).
[31] W. Borcherds, A. Bremer, M. B. Borgia, and T. Mittag, How do intrinsically disordered protein regions encode a driving force for liquid–liquid phase separation?, Curr. Opin. Struct. Biol. **67**, 41 (2021).
[32] S. B. Shuker, P. J. Hajduk, R. P. Meadows, and S. W. Fesik, Discovering high-affinity ligands for proteins: SAR by NMR, Science **274**, 1531 (1996).
[33] E. T. Mack, P. W. Snyder, R. Perez-Castillejos, and G. M. Whitesides, Using covalent dimers of human carbonic anhydrase II to model bivalency in immunoglobulins, J. Am. Chem. Soc. **133**, 11701 (2011).
[34] A. Whitty, Cooperativity and biological complexity, Nat. Chem. Biol. **4**, 435 (2008).
[35] Q. L. Lei, C. L. Ren, X. H. Su, and Y. Q. Ma, Crowding-induced cooperativity in DNA surface hybridization, Sci. Rep. **5**, 1 (2015).
[36] E. N. Kaufman and R. K. Jain, Effect of bivalent interaction upon apparent antibody affinity: Experimental confirmation of theory using fluorescence photobleaching and implications for antibody binding assays, Cancer Res. **52**, 4157 (1992), https://aacrjournals.org/cancerres/article/52/15/4157/497901/Effect-of-Bivalent-Interaction-upon-Apparent.
[37] J. A. Reynolds, Interaction of divalent antibody with cell surface antigens, Biochemistry **18**, 264 (1979).
[38] See Supplemental Material http://link.aps.org/supplemental/10.1103/PhysRevLett.130.258401, which includes Refs. [5,24,39–49], for details of calculations of concentration profiles, statistical mechanics of chemical equilibrium in crowded environments (including scaled particle theory, Brownian dynamics and Monte Carlo simulations, and the derivation of Eq. (6)), details of the IgG model, and supplementary plots.
[39] D. J. Diestler and E. W. Knapp, Statistical mechanics of the stability of multivalent ligand-receptor complexes, J. Phys. Chem. C **114**, 5287 (2010).
[40] T. Ando and J. Skolnick, Crowding and hydrodynamic interactions likely dominate *in vivo* macromolecular motion, Proc. Natl. Acad. Sci. U.S.A. **107**, 18457 (2010).
[41] E. Słyk, T. Skóra, and S. Kondrat, A minimal coarse-grained model for Immunoglobulin G (IgG): Diffusion and binding under crowding (to be published).
[42] L. Bongini, D. Fanelli, F. Piazza, P. De Los Rios, S. Sandin, and U. Skoglund, Freezing immunoglobulins to see them move, Proc. Natl. Acad. Sci. U.S.A. **101**, 6466 (2004).
[43] R. M. Gibbons, The scaled particle theory for particles of arbitrary shape, Mol. Phys. **17**, 81 (1969).
[44] G. A. Huber and J. A. McCammon, Brownian dynamics simulations of biological molecules, Trends Chem. **1**, 727 (2019).
[45] E. O. Saphire, P. W. Parren, R. Pantophlet, M. B. Zwick, G. M. Morris, P. M. Rudd, R. A. Dwek, R. L. Stanfield, D. R. Burton, and I. A. Wilson, Crystal structure of a neutralizing human IgG against HIV-1: A template for vaccine design, Science **293**, 1155 (2001).

[46] H. M. Berman, J. Westbrook, Z. Feng, G. Gilliland, T. N. Bhat, H. Weissig, I. N. Shindyalov, and P. E. Bourne, The protein data bank, Nucl. Acids Res. **28**, 235 (2000).
[47] D. Sehnal, S. Bittrich, M. Deshpande, R. Svobodová, K. Berka, V. Bazgier, S. Velankar, S. K. Burley, J. Koča, and A. S. Rose, Mol* viewer: Modern web app for 3D visualization and analysis of large biomolecular structures, Nucl. Acids Res. **49**, W431 (2021).
[48] M. Chen and K. Y. Lin, Universal amplitude ratios for three-dimensional self-avoiding walks, J. Phys. A **35**, 1501 (2002).
[49] M. Rubinstein and R. H. Colby, *Polymer Physics* (Oxford University Press, New York, 2003), pp. 102–104.
[50] W. F. Mangel, B. Lin, and V. Ramakrishnan, Characterization of an extremely large, ligand-induced conformational change in plasminogen, Science **248**, 69 (1990).
[51] M. Tsytlonok, K. Hemmen, G. Hamilton, N. Kolimi, S. Felekyan, C. A. Seidel, P. Tompa, and H. Sanabria, Specific conformational dynamics and expansion underpin a multi-step mechanism for specific binding of p27 with Cdk2/Cyclin A, J. Mol. Biol. **432**, 2998 (2020).
[52] C. A. Pickover, D. B. McKay, D. M. Engelman, and T. A. Steitz, Substrate binding closes the cleft between the domains of yeast phosphoglycerate kinase, J. Biol. Chem. **254**, 11323 (1979).
[53] S. A. Kumar, N. S. Murthy, and J. S. Krakow, Ligand-induced change in the radius of gyration of cAMP receptor protein from Escherichia coli, FEBS Lett. **109**, 121 (1980).
[54] M. E. Newcomer, B. A. Lewis, and F. A. Quiocho, The radius of gyration of L-arabinose-binding protein decreases upon binding of ligand, J. Biol. Chem. **256**, 13218 (1981).
[55] C. Dumas and J. Janin, Conformational changes in arginine kinase upon ligand binding seen by small-angle x-ray scattering, FEBS Lett. **153**, 128 (1983).
[56] B. Shaanan, Structure of human oxyhaemoglobin at $2 \cdot 1$ resolution, J. Mol. Biol. **171**, 31 (1983).
[57] G. A. Olah, S. Trakhanov, J. Trewhella, and F. A. Quiocho, Leucine/isoleucine/valine-binding protein contracts upon binding of ligand, J. Biol. Chem. **268**, 16241 (1993).
[58] T. C. Taylor and I. Andersson, Structural transitions during activation and ligand binding in hexadecameric Rubisco inferred from the crystal structure of the activated unliganded spinach enzyme, Nat. Struct. Biol. **3**, 95 (1996).
[59] M. Sevvana, V. Vijayan, M. Zweckstetter, S. Reinelt, D. R. Madden, R. Herbst-Irmer, G. M. Sheldrick, M. Bott, C. Griesinger, and S. Becker, A ligand-induced switch in the periplasmic domain of sensor histidine kinase CitA, J. Mol. Biol. **377**, 512 (2008).
[60] M. Salvi, B. Schomburg, K. Giller, S. Graf, G. Unden, S. Becker, A. Lange, and C. Griesinger, Sensory domain contraction in histidine kinase CitA triggers transmembrane signaling in the membrane-bound sensor, Proc. Natl. Acad. Sci. U.S.A. **114**, 3115 (2017).
[61] S. Ghobadi, M. R. Ashrafi-Kooshk, H. Mahdiuni, and R. Khodarahmi, Enhancement of intrinsic fluorescence of human carbonic anhydrase II upon topiramate binding: Some evidence for drug-induced molecular contraction of the protein, Int. J. Biol. Macromol. **108**, 240 (2018).
[62] D. J. Diestler and E. W. Knapp, Statistical Thermodynamics of the Stability of Multivalent Ligand-Receptor Complexes, Phys. Rev. Lett. **100**, 178101 (2008).
[63] R. Cheng, Conformational dynamics of an unfolded biopolymer: Theory and simulation, Ph.D. thesis, 2012.
[64] The gyration radius of the linear chain agrees well with that of a self-avoiding random walk on a BCC lattice in 3D (Fig. S3).
[65] M. Grimaldo, H. Lopez, C. Beck, F. Roosen-Runge, M. Moulin, J. M. Devos, V. Laux, M. Härtlein, S. Da Vela, R. Schweins, A. Mariani, F. Zhang, J.-L. Barrat, M. Oettel, V. T. Forsyth, T. Seydel, and F. Schreiber, Protein short-time diffusion in a naturally crowded environment, J. Phys. Chem. Lett. **10**, 1709 (2019).
[66] S. Kondrat, O. Zimmermann, W. Wiechert, and E. von Lieres, The effect of composition on diffusion of macromolecules in a crowded environment, Phys. Biol. **12**, 046003 (2015).
[67] T. Frembgen-Kesner and A. H. Elcock, Striking effects of hydrodynamic interactions on the simulated diffusion and folding of proteins, J. Chem. Theory Comput. **5**, 242 (2009).
[68] T. Miyaguchi, Reduction of self-diffusion coefficient in a coarse-grained model of cytoplasm, Phys. Rev. Res. **2**, 013279 (2020).